Ocean Heat Flux in the Central Weddell Sea during Winter

MILES G. MCPHEE

McPhee Research Company, Naches, Washington

CHRISTOPH KOTTMEIER

Institut fuer Meteorologie und Klimaforschung, Universitaet Karlsruhe, Karlsruhe, Germany

JAMES H. MORISON

Polar Science Center, University of Washington, Seattle, Washington

(Manuscript received 14 January 1998, in final form 19 June 1998)

ABSTRACT

Seasonal sea ice, which plays a pivotal role in air–sea interaction in the Weddell Sea (a region of large deep-water formation with potential impact on climate), depends critically on heat flux from the deep ocean. During the austral winter of 1994, an intensive process-oriented field program named the Antarctic Zone Flux Experiment measured upper-ocean turbulent fluxes during two short manned ice-drift station experiments near the Maud Rise seamount region of the Weddell Sea. Unmanned data buoys left at the site of the first manned drift provided a season-long time series of ice motion, mixed layer temperature and salinity, plus a (truncated) high-resolution record of temperature within the ice column. Direct turbulence flux measurements made in the ocean boundary layer during the manned drift stations were extended to the ice–ocean interface with a ''mixing length'' model and were used to evaluate parameters in bulk expressions for interfacial stress (a ''Rossby similarity'' drag law) and ocean-to-ice heat flux (proportional to the product of friction velocity and mixed layer temperature elevation above freezing). The Rossby parameters and dimensionless heat transfer coefficient agree closely with previous studies from perennial pack ice in the Arctic, despite a large disparity in undersurface roughness. For the manned drifts, ocean heat flux averaged 52 W m^{-2} west of Maud Rise and 23 W m^{-2} over Maud Rise. Unmanned buoy heat flux averaged 27 W m^{-2} over a 76-day drift. Although short-term differences were large, average conductive heat flux in the ice was nearly identical to ocean heat flux over the 44-day ice thermistor record.

1. Introduction

Deep waters of the World Ocean are linked to the rest of the climate system in limited geographical regions confined to high latitudes. The connection is thought to be especially strong in the Weddell Sea (Gordon 1991). Near the Antarctic continental margin, cold, saline water is produced by katabatic winds that blow the insulating sea ice cover offshore, providing an annual pulse of dense water capable of migrating down the slope and mixing to form bottom and deep waters (Gill 1973). A less predictable but potentially important source of deep water is direct cooling by deep convection away from the continental shelves. The water column in the central and eastern part of the Weddell is often only marginally stable, with a potentially powerful source of negative surface buoyancy associated with salt rejection during ice growth.

In the mid-1970s, a large expanse of open water (or very low sea ice concentration) persisted through several austral winters, far removed from both continental and sea ice margins (Zwally and Gloersen 1977; Carsey 1980). During its active period, the Weddell polynya, which occupied as much as 10% of the area of the Weddell gyre, significantly cooled the deep waters of the Weddell (Gordon 1991) and may have contributed several times as much to deep-water formation as the continental shelves (Gordon 1982). Direct evidence of deep convection was observed in remnant convective ''chimneys'' (Gordon 1978). The Weddell polynya apparently represented a quasi-stable mode in which deep convection forced strong vertical fluxes of heat and salt and prevented formation of the seasonal ice cover (Martinson et al. 1981). There is naturally much interest in what conditions might again lead to persistent deep convection, eliminating the annual sea ice cover in the region and cooling the deep ocean.

Corresponding author address: Miles G. McPhee, 450 Clover Springs Road, Naches, WA 98937.
E-mail: miles@apl.washington.edu

The state of the sea ice cover of the Southern Ocean is intricately tied to heat loss from the deep ocean, which occurs mainly during winter. This contrasts sharply with the perennial pack of the Arctic, where ocean-to-ice heat transfer results mostly from summer solar heating through open leads and thin ice (Maykut and McPhee 1995). Even prior to direct flux measurements made in the Weddell during the Antarctic Zone Flux Experiment (ANZFLUX; see McPhee et al. 1996), there was strong inferential evidence for relatively large heat flux into the mixed layer from below, including (i) late winter ice thickness of only 0.6–0.7 m (Wadhams et al. 1987); (ii) persistent elevation of mixed layer temperature above freezing (Gordon and Huber 1984, 1990); and (iii) entrainment of geochemical tracers (Gordon and Huber 1990; Schlosser et al. 1990). Gordon and Huber, for example, found the average temperature elevation above freezing to be about 0.08 K and used oxygen undersaturation to infer an average winter heat flux into the mixed layer from below of around 40 W m^{-2} along the Greenwich meridian from 60° to 70°S. The inferred heat flux increased from north to south, that is, with penetration into the ice pack. Heat flux of this magnitude prevents sea ice growth at a rate of about 2 cm day^{-1}, which would otherwise inject enough salt into the mixed layer to destabilize the water column, over much of the Weddell Sea.[1]

In general, numerical modeling results (Washington et al. 1976; Martinson 1990) have found that significantly more oceanic heat flux is required to explain the seasonal evolution of the ice cover in the Weddell Sea compared with the average 2 W m^{-2} needed for equilibrium in the thermodynamic model of the Arctic ice pack developed by Maykut and Untersteiner (1971). An exception is the study of Lemke et al. (1990), who used a coupled thermodynamic–dynamic ice model and ocean mixed layer model to compute an average heat flux over their Weddell Sea domain of about 3 W m^{-2}. In their model, the highest flux occurs during the summer and near the periphery of the ice pack. Over most of the ice-covered domain, the oceanic heat flux was around 2 W m^{-2}, which is at odds in both temporal and spatial distribution with observations of Gordon and Huber (1984, 1990).

The aim of ANZFLUX was to drive the research icebreaker *Nathaniel B. Palmer* deep into the winter ice pack of the Weddell Sea in order to measure the response of the ice–ocean system to storm events. A specific goal was to measure oceanic heat flux and Reynolds stress near the ice–ocean interface to confirm that large oceanic heat flux events did in fact occur. We also hoped to relate the fluxes to more easily measured variables, such as ice velocity and temperature elevation of the mixed layer. Given plausible exchange coefficients, it would then be possible to determine ice–ocean fluxes from unmanned buoy measurements over much larger scales and longer times. The objective of this paper is to carry out this strategy using the ANZFLUX data. Flux measurements from the manned drift stations are analyzed and extrapolated to the ice–ocean interface in the context of a model for turbulent exchange. Exchange coefficients are derived from these data, then used to compute average fluxes during the manned drifts, and also applied to data from a buoy cluster left to drift at the site of the first manned station. The buoy data thus provide estimates of mean heat flux from the ocean, as well as through the ice cover, over most of the austral 1994 winter season in the area immediately west and north of Maud Rise.

2. The experiment

The ANZFLUX experiment is described by McPhee et al. (1996). The ship supported two separate manned drift stations, each lasting about 6 days. The first, referred to as the Warm Regime Station (WRS), was deployed about 400 km southwest of Maud Rise in a region of relatively high maximum temperature (T_{max}) in the water column. It its short life it drifted more than 150 km in response to two intense cyclones, each with peak sustained surface winds approaching 20 m s^{-1}. During the drift, warm core eddies were encountered, with large excursions in the depth of the pycnocline and episodes of large heat flux in the mixed layer (McPhee et al. 1996). Ice deformation during the second storm forced evacuation earlier than planned; however, an unmanned buoy cluster (described below) was deployed at the site before the ship departed for the second drift site over Maud Rise, a bathymetric feature centered at about 64°30′S, 3°E rising about 2 km above the surrounding abyssal plain. In the 1970s, the Weddell polynya first appeared over Maud Rise, then drifted slowly westward. During the Maud Rise Station, storms were less energetic, and T_{max} was about 0.5 K lower than to the west. Nevertheless, there were comparable excursions in the depth of the pycnocline and large variations in mixed layer heat flux.

The manned drift stations included instrument systems for measuring turbulent fluxes at several levels in the ocean boundary layer, as well as mean currents (via acoustic Doppler current profilers) and high-resolution temperature, salinity, and microstructure profiles. Fluxes of momentum (Reynolds stress: $\langle \mathbf{u}'w' \rangle$ where $\mathbf{u}'$ is the horizontal deviatory velocity vector and w' is vertical velocity) and sensible heat ($\rho c_p \langle w'T' \rangle$, where ρ is density, c_p is specific heat for seawater, and T' is deviatory temperature) were measured with *turbulence instrument clusters* (TICs) mounted at fixed levels on a rigid mast

[1] From a one-dimensional, static stability standpoint, however, heat entrained by incipient deep convection would rapidly melt ice and "cap" convection. Sustained deep convection requires that the negative buoyancy flux associated with surface cooling, net ice export, and salinity flux divergence in the mixed layer outweigh the positive buoyancy flux from melting, until the ice is gone.

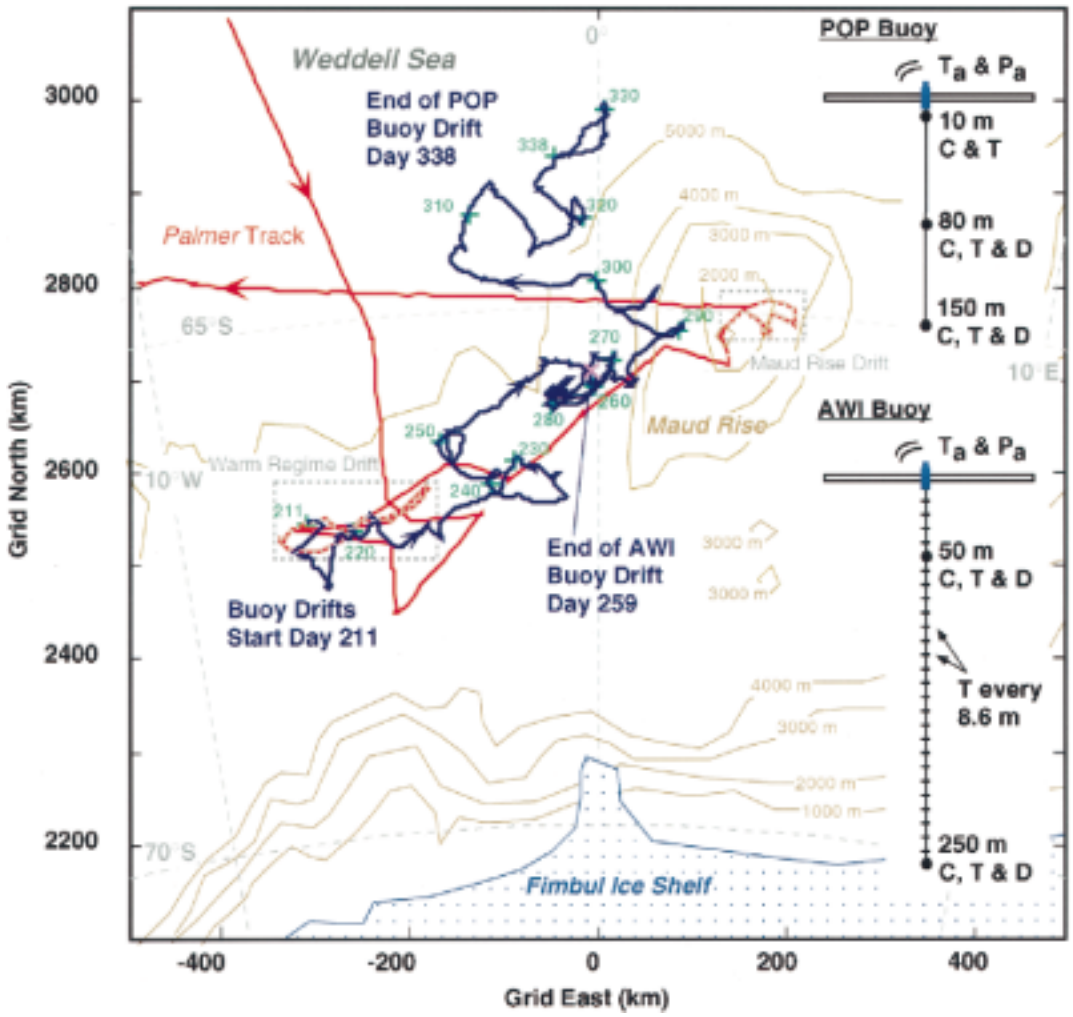

FIG. 1. Drift track of the ANZFLUX buoy cluster. The buoys were deployed at the ANZFLUX Warm Regime drift station on 30 Jul 1994 (day 211). The track is shown in blue with a "+" marker every 10 days. The cruise tract of the *Nathaniel B. Palmer* is shown in red. The AWI buoy functioned until 16 Sep (day 259). The POP buoy drifted over the flank of Maud Rise, then north until it ceased reporting on 6 Dec (day 338).

that could be lowered as a unit to any level in the boundary layer. Each TIC comprises three small, partially ducted mechanical current meters mounted along mutually orthogonal axes canted 45° to the horizontal, mounted near fast response thermistors and ducted conductivity meters. The system is described in detail by McPhee (1992) and McPhee and Stanton (1996). Two separate masts were deployed at each station. The turbulent flux data were supplemented by temperature and salinity profiles from an automated microstructure profiler (Stanton 1995) that furnished a high-resolution view of the mean *T–S* structure in the upper ocean.

Unmanned drifting buoys provided the long time series component of the ANZFLUX measurement program. These included two multisensor buoys deployed at the WRS, a thermistor buoy from the Alfred Wegener Institute (AWI) and a Polar Ocean Profile (POP) hydrographic buoy built by the Applied Physics Laboratory at the University of Washington. Both buoys employ aluminum tube hulls that are installed through holes in the ice. The hulls contain data processing electronics and Argos transmitters, with enough batteries to operate for two years. Electronic systems within the buoys collect and process the sensor data and transmit them via satellite through the Argos system. Both buoys measure air temperature with thermistors contained in radiation-shielded and self-aspirated housings about 1 m above the ice surface, along with atmospheric pressure using accurate and stable quartz pressure sensors. Each buoy supports an array of different but complementary ocean sensors.

As illustrated in the inset of Fig. 1, the AWI buoy supports a thermistor string 250 m in length with a sensor separation of 8.6 m. The string also carries Sea-Bird conductivity–temperature–depth instruments (CTD) at depths of 50 and 250 m. The depths of the

thermistors are estimated from the CTD data and a theoretical cable catenary model. A second thermistor string 2 m long with a sensor separation of 10 cm is installed in the ice near the buoy to obtain information on snow and sea ice thickness changes and ice heat flux. The data processing electronics average the information from the ocean sensors over 10 minutes and transmit the averages through the Argos system.

The sensor layout of the POP buoy is also illustrated in Fig. 1. A similar buoy was used previously in the western Weddell Sea as part of the 1992 Ice Station Weddell project (Levine et al. 1997). The buoy supports a cable 150-m long with Sea-Bird SBE-16 CTD instruments mounted at 10 m, 80 m, and 150 m. In operation these are queried every 12 minutes by the data processing electronics and the temperature and salinity data are transmitted through the Argos satellite system.

The drift track of the AWI and POP buoy cluster is shown, along with the cruise track of the *Nathaniel B. Palmer*, in Fig. 1. The buoys were installed at the WRS drift site on 30 July 1994 (day 211). They drifted together until AWI buoy ceased functioning on 16 September (day 259). The POP buoy continued from the WRS drift site, northeast to Maud Rise over a period of about 2.5 months. It then drifted north and slightly west into open water conditions around 28 November and ceased transmitting 6 December 1994 (day 338). Data suggest the POP buoy failed after being subjected to large waves in the marginal ice zone.

3. Transfer coefficients

The transfer of heat from the mixed layer to sea ice depends on both the turbulent stress at the ice–ocean interface, characterized by the friction speed u_{*0}, equal to the square root of kinematic stress at the interface, and the available heat content of fluid in the turbulent boundary layer, which is approximately proportional to the elevation of mixed layer temperature above freezing, $\delta T = T_{\rm ml} - T_f(S_{\rm ml})$, where T_f is the freezing temperature (at surface pressure) for mixed layer salinity $S_{\rm ml}$ (McPhee et al. 1987; McPhee 1990, 1992, 1994). The kinematic heat flux at the ice–water interface $\langle w'T'\rangle_0$ may be expressed in terms of a heat transfer coefficient c_H (a turbulent Stanton number) according to

$$\langle w'T'\rangle_0 = c_H u_{*0}\delta T. \qquad (1)$$

To estimate interfacial heat flux without detailed flux measurements thus requires knowledge of both u_{*0} and c_H. The purpose of this section is to utilize flux measurements taken during the manned station phase of ANZFLUX to derive parameters needed to express (1) in terms of quantities accurately measured by the unmanned buoy cluster, namely, ice velocity and mixed layer temperature and salinity.

Determining u_{*0} from ice velocity (relative to ocean current at the far extent of the frictional boundary layer) is directly analogous to determining the surface wind stress from the geostrophic wind aloft. A framework called Rossby-similarity theory provides a practical way of expressing the ratio of ice velocity (relative to geostrophic ocean current due to sea surface tilt) to surface friction velocity (McPhee 1979, 1990). It can be expressed compactly using complex numbers for horizontal vectors. Let $\mathbf{U}_0 = \mathbf{U}_i - \mathbf{U}_g$ be the vector ice (surface) velocity relative to surface geostrophic current in the ocean $\mathbf{U}_g$, and let $\mathbf{u}_{*0}$ be the surface friction *velocity*, that is, a vector in the direction of interfacial stress with magnitude equal to its square root. The Rossby-similarity drag law is

$$\hat{\Gamma} = \frac{\mathbf{U}_0}{\mathbf{u}_{*0}} = \frac{1}{\kappa}(\log(\mathrm{Ro}_*) - A - i\,\mathrm{sgn}(f)B), \qquad (2)$$

where i is the imaginary number, f is the Coriolis parameter (negative in the Southern Hemisphere), A and B are the Rossby-similarity parameters, and $\mathrm{Ro}_* = u_{*0}/(|f|z_0)$ is the surface friction Rossby number. The dimensionless surface velocity $\hat{\Gamma}$ is complex because surface velocity and interfacial stress are not in general aligned. Here Ro_* depends on the *surface* roughness length z_0, which derives from the integration constant for the logarithmic current profile observed near the surface in the planetary boundary layer (PBL). For surfaces with relatively uniform roughness elements, as found in typical laboratory flows, z_0 is about 1/30 of the scale of the roughness elements. The spectrum of undersurface roughness for sea ice is broad; hence the meaning of z_0 is more abstract. It is found to vary widely, depending on ice thickness, age, location, and deformation history. Observations range from hydraulically smooth ($\sim 0.1\nu/u_{*0}$, where ν is kinematic molecular viscosity) to around 0.1 m (McPhee 1990), a span of nearly four orders of magnitude.

Laboratory studies suggest that c_H may also depend on z_0. Owen and Thompson (1963) and Yaglom and Kader (1974, hereafter YK) studied turbulent heat transfer across hydraulically rough surfaces and found the turbulent Stanton number to vary approximately as the inverse square root of the *roughness* Reynolds number based on the thickness of a *transition sublayer* comparable to the roughness element scale $\mathrm{Re} = u_{*0}h_{\rm sl}/\nu$, where $h_{\rm sl} = 30z_0$. If the laboratory results were directly applicable to sea ice, c_H might also be expected to vary widely, perhaps by as much as two orders of magnitude. Instead, it appears to be quite uniform, ranging from about 0.005 to 0.006 (McPhee 1992). An important facet of the ANZFLUX experiment was to test whether the comparatively smooth seasonal ice of the eastern Weddell exhibited a correspondingly larger value of c_H than the multiyear pack of the Arctic and western Weddell.

With continuous measurements of ice velocity (via satellite navigation) and mixed layer temperature and salinity (and provided $\mathbf{U}_g$ can be estimated or is small enough to be ignored relative to $\mathbf{U}_i$), heat flux is obtained by combining (1) and (2):

$$H = \rho c_p \frac{U_0}{\Gamma} c_H (T_{\rm ml} - T_f), \qquad (3)$$

where U_0 and Γ are magnitudes of the respective complex (vector) quantities. It remains to evaluate the parameters A, B, z_0, and c_H characteristic of the region being considered, using turbulent momentum and heat flux data gathered during the ANZFLUX manned drift stations.

a. Undersurface roughness length

In the atmospheric boundary layer, turbulent stress is usually measured close enough to the surface to be considered within the ''constant flux'' surface layer and is assumed to be the same as surface stress. The standard measurement height of 10 m might typically represent 1% or less of the total boundary layer extent. In the ocean, measurement depth is often an appreciable fraction of PBL depth, thus a model is required for extrapolating stress measured at a particular level to the boundary at the ice–ocean interface. The approach taken here is based on the mixing length algorithm of McPhee (1994), adapted to a steady-state model for eddy viscosity that depends on specified surface stress and buoyancy flux, and on mean temperature and salinity profiles (McPhee 1999). The model works by (i) ignoring local inertia in the PBL momentum equation, (ii) determining the maximum mixing length in the mixed layer based on surface stress and buoyancy flux conditions, (iii) making an initial guess at the distribution of u_* (the square root of local Reynolds stress) based on the Ekman solution of the turbulent stress equation (McPhee and Martinson 1994), then (iv) iterating to a solution that includes the effect of density gradients below the mixed layer. The iteration continues until the difference between observed and modeled u_* at the measurement level is smaller than some specified tolerance. The mixed layer depth is defined by the region in the model domain above which the squared buoyancy frequency is less than a prescribed limit, in the present case $N^2 = -(g/\rho)\rho_z < 1 \times 10^{-6}$ s^{-2}, where g is the acceleration of gravity, ρ is density, and ρ_z its vertical gradient. Surface buoyancy flux is obtained by using a Stanton number approach (see section 3c) to estimate heat flux at the ice–water interface, then combining it with the conductive heat flux through the ice to get the melt rate and salinity flux (McPhee 1990). At low temperatures buoyancy is controlled mainly by salinity.

Given modeled profiles of friction velocity and eddy viscosity, z_0 is determined as shown schematically in Fig. 2. In a reference frame where $\mathbf{u}_{*0}$ is aligned with the real axis, the uppermost grid level in the model (zz_1) is chosen to be close enough to the solid surface so that the velocity difference between it and the surface is also real. By the geometry illustrated, the modeled velocity difference between the turbulence cluster measurement level and the surface is the negative of the observed velocity ($\hat{\mathbf{u}}_{\rm rel}$) measured in a reference frame attached to the ice. The method furnishes both z_0 and the direction of $\mathbf{u}_{*0}$ in geographic coordinates based on the direction of the measured relative current.

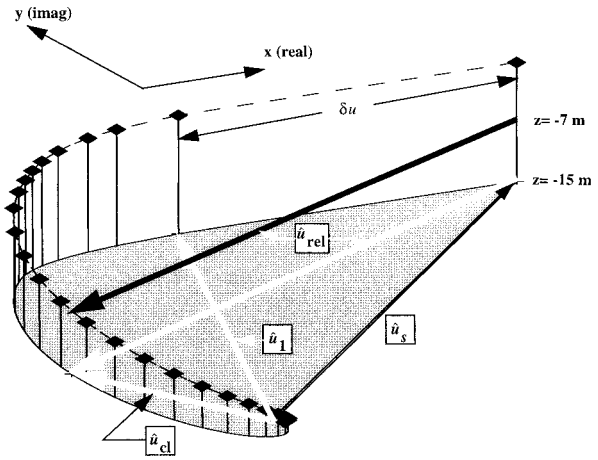

$\hat{u}_s$ surface (ice) velocity
$\hat{u}_1$ model velocity, at topmost level in the model, zz_1
$\hat{u}_{\rm cl}$ model velocity, at cluster measurement level
$\hat{u}_{\rm rel}$ relative velocity between surface and measurement level
S measured current speed at cluster level, $S = |\hat{u}_{\rm rel}|$
δu change in velocity from zz_1 to surface, real if surface stress is along real axis

$$Im(\hat{u}_{\rm rel}) = Im(\hat{u}_1 - \hat{u}_{\rm cl})$$
$$Re(\hat{u}_{\rm rel}) = Re(\hat{u}_1 - \hat{u}_{\rm cl}) + \delta u$$
$$\log z_0 = \log|zz_1| - \frac{\kappa \delta u}{u_{*0}}$$

FIG. 2. Schematic illustrating the steps used in evaluating surface roughness z_0 and the direction of the surface friction velocity. The model is solved for Reynolds stress and absolute velocity on a grid with the topmost level near the surface, using stress measurements at one level (here, 7 m below the ice). A geometric construction is then used as shown to relate current speed measured relative to the ice at the measurement level, to the shear between the ice and the first gridpoint, from which z_0 is determined from the law of the wall.

If measurements are made near the solid surface, it is often acceptable to use the ''constant stress'' assumption as in the atmospheric surface layer, and to get $\log z_0$ directly from integration of the dimensionless shear equations of Monin–Obukhov similarity theory. The method here is more general, allowing for measurements well beyond the constant stress layer and lessening the impact of surface inhomogeneity. The strategy chosen for determining z_0 was to use the best available data at any particular time for determining surface fluxes. Turbulence data were screened for quality, then grouped in ''15-min realizations'' for calculating covariance friction velocity and heat flux: $u_* = (\langle u'w' \rangle^2 + \langle v'w' \rangle^2)^{1/4}$ and $H = \rho c_p \langle w'T' \rangle$ (see McPhee 1992, 1994) for times when one or more clusters pro-

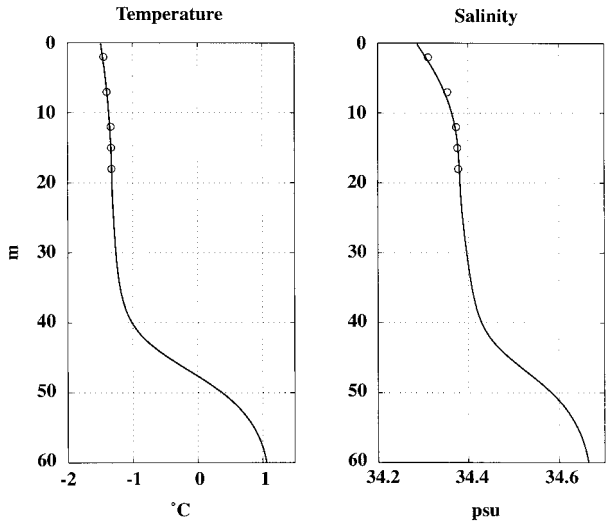

FIG. 3. Average upper-ocean temperature and salinity profiles for the 2.4-h period centered at day 207.55. Solid curves are from the Loose-tethered Microstructure Profile (courtesy of T. Stanton). Symbols are from fixed levels of the turbulence instrument cluster mast.

vided good data in the upper 10 m of the water column. The flux and mean data were then averaged in 0.1 day (2.4 h) bins. High-resolution temperature and salinity profiles from the Loose-tethered Microstructure Profiler (LMP) (T. Stanton 1996, personal communication) were similarly averaged during times when the two systems operated simultaneously.

An example taken from a relatively low-stress, 2.4-h data segment as the WRS drifted over a warm eddy illustrates the PBL model application during a time when there was significant stress attenuation and Ekman turning in the upper 10 m of the water column. Figure 3 shows mean temperature and salinity profiles from the LMP, along with corresponding data at fixed levels from five TICs on the ''A mast.'' There was stratification in the upper 10 m, and mixed layer temperature was well above freezing. TICs were located at 2, 7, 12, 15, and 18 m below the interface. Reynolds stress measured with the second cluster (7 m) was used to force the model along with the density structure corresponding to the observed T and S profiles. Surface buoyancy flux was obtained from the heat and mass balance at the interface, with conductive heat flux in the sea ice estimated to be 30 W m^{-2} based on its measured temperature gradient (McPhee et al. 1996). Model computed quantities are compared with observed in Fig. 4. The model is forced to coincide with observed at 7 m; it also agrees reasonably well at the other measurement depths. Computed values for u_{*0} and z_0 are 8.8×10^{-3} m s^{-1} and 0.9 mm. While normally the TIC at 2 m would be a better choice to represent surface conditions, in this case it makes little difference since the model predicts conditions at both levels about equally well. Using the deeper cluster shows how flux measured well away from the surface (Reynolds stress at 7 m is about 20% of the surface value) can be extrapolated to the interface. The current hodograph used to illustrate the method for finding z_0 in Fig. 2 was taken from this example with $\hat{\mathbf{u}}_{\text{rel}}$ being the measured velocity 7 m below the ice and $zz_1 = -0.15$ m.

At the WRS there were 20 suitable 2.4-h averages for determining surface fluxes. Of these 13 were accompanied by LMP T and S profiles, which included all segments for which there was any indication of mixed layer density gradient in the TIC data. At other

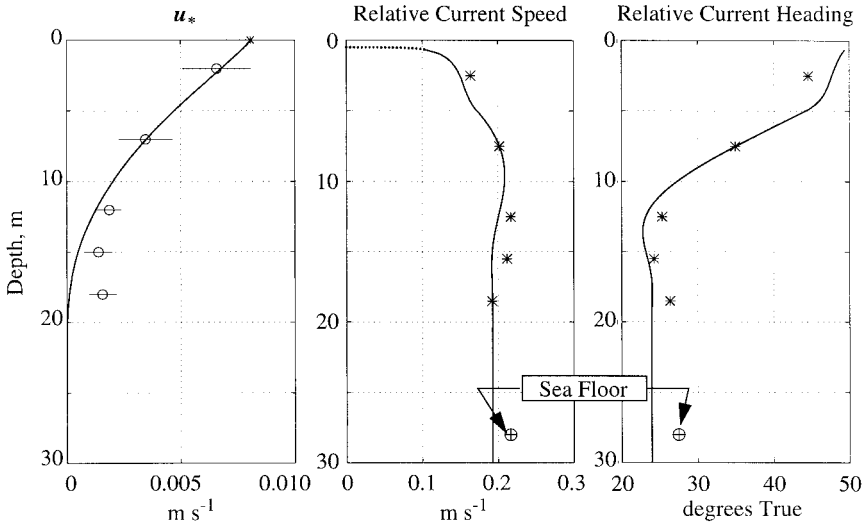

FIG. 4. Model results obtained by forcing the model to match the Reynolds stress and current velocity measured 7 m below the ice, compared with data from the remaining four TICs in the boundary layer. Also shown is the apparent speed and heading of the sea floor, relative to the drifting reference frame.

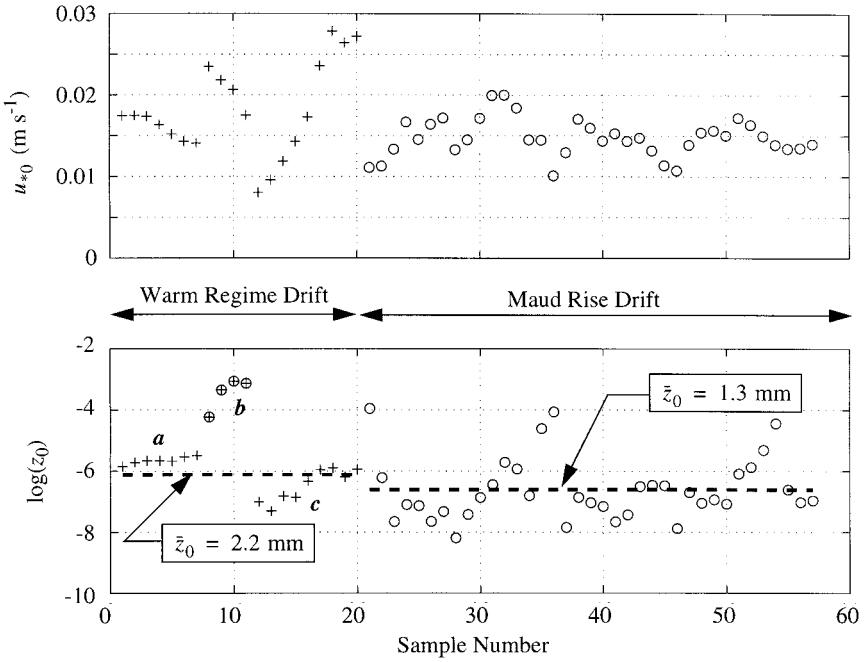

FIG. 5. Interfacial friction velocity and surface roughness determined for each of the 2.4-h segments with suitable turbulence data at the manned drift stations. The data group labeled ***b*** were from a time of extreme changes in mixed layer structure and were not used in estimating the mean surface roughness.

times the mixed layer was assumed isopycnal and 100 m deep. At the Maud Rise station, one TIC at 3-m depth on a rigid mast suspended directly from the ice provided the surface flux conditions. Extreme conditions of stratification and warming like those seen during the WRS were not encountered over Maud Rise. Results of the u_{*0} and z_0 determinations for all the data segments are summarized in Fig. 5. At the WRS site, there were three distinct data groupings. The two labeled ***a*** and ***c*** in the plot were from different masts in different locations separated by about 70 m. The four data segments labeled ***b*** came during the time in the first gale (day 206) when the station was drifting onto the warm eddy (see Fig. 5 of McPhee et al. 1996). The wind was quite strong, the mixed layer was shoaling rapidly, and upward heat flux was extreme in the warm water overlying the eddy. Conditions were so anomalous that these segments were not included in deriving the average drag and heat flux parameters. With these exclusions, averaging logz_0 for each station implies undersurface roughness scales of 2.2 mm (with a range from 1.2 to 3.9 mm associated with ± 1 standard deviation of the logz_0 series) and 1.3 mm (range, 0.5–3.8 mm) for the Warm Regime and Maud Rise stations, respectively. Given the same ice speed, the difference in mean z_0 at the two stations would cause a variation in u_{*0} of about 5%.

b. Rossby similarity parameters

The similarity parameters in (2) were determined by averaging ice drift velocity obtained from accurate satellite navigation in the same 0.1-d segments, then for each segment dividing the complex drift velocity by the complex friction velocity determined from the modeling discussed in section 3a: $\hat{\Gamma} = \mathbf{U}_0/\mathbf{u}_{*0}$. This was done for the WRS drift only since direction control by flux-gate compasses on masts A and B was superior to the ice-suspended cluster at the Maud Rise site. Given a series of the nondimensional ice velocity, A and B are estimated from

$$B = \overline{\kappa \mathrm{Im}(\hat{\Gamma})}$$
$$A = \overline{\kappa \mathrm{Re}(\hat{\Gamma}) - \log z_0}, \qquad (4)$$

where the overbars represent averaging over the sample series. It is tacitly assumed in this calculation that the ice velocity is nearly the same as the change in velocity across the boundary layer if enough samples are averaged. From comparing ice drift with deeper currents measured by acoustic Doppler current profiler (data courtesy of R. Muench 1995, personal communication), it was clear that both tidal flow and geostrophic shear were often present in the upper ocean during ANZFLUX. There was, however, little evidence of a persistent geostrophic (sea surface tilt) flow that would contaminate the averages in (4), which are $A = 2.0$ and $B = 2.5$. These agree reasonably well with the empirical AIDJEX results, $A = 1.91$ and $B = 2.12$ of McPhee (1979), and the theoretical result, $A = 2.2$ and $B = 2.3$ of McPhee (1990). Undersurface roughness was about 50–100 times larger at the AIDJEX sites. Since the turn-

ing angle is typically 30° or less, variation in B has little impact on the magnitude of $\hat{\Gamma}$.

c. Heat transfer coefficient

Previous ice station results (McPhee 1992) show that kinematic heat flux at the ice–ocean interface depends mainly on the friction velocity and mixed layer temperature elevation above freezing. It may also depend to a lesser extent on surface roughness and molecular viscosity (YK; McPhee et al. 1987):

$$\langle w'T' \rangle = f(\nu, z_0, \delta T, u_{*0}). \tag{5}$$

Dimensional analysis provides a way of testing the Reynolds number dependency for the relatively smooth ice of the eastern Weddell. Of the four governing parameters on the right-hand side of (5), three are dimensionally independent; thus according to the Π theorem, one dimensionless group formed from the parameters may be expressed as a function of a second dimensionless group (e.g., Barenblatt 1996):

$$\frac{\langle w'T' \rangle}{u_{*0}\delta T} = f\left(\frac{u_{*0}z_0}{\nu}\right). \tag{6}$$

The left-hand side of (6) is the nondimensional heat flux, a Stanton number based on friction speed instead of mean speed, while the dimensionless group on the right side is a Reynolds number based on roughness length and friction speed, and (6) is thus $\mathrm{St}_* = f(\mathrm{Re}_*)$.[2] If the right-hand side turns out to be nearly constant, then neglecting z_0 and ν in the parameter list of (5) is justified. Using data from both drifts, but excluding extreme conditions and periods of negative heat flux during the drift onto and off of the warm eddy, 47 averages (2.4 h each) of near-surface $\langle w'T' \rangle$, u_{*0}, z_0, and mixed layer δT are available for analysis and are plotted as a scatter diagram of St_* versus Re_* in Fig. 6a. A least squares fit linear regression is shown by the heavy dashed line, the equation of which is

$$\mathrm{St}_* = (0.0058 \pm 0.0004) + (-1.0 \pm 1.2) \times 10^{-5}\mathrm{Re}_*, \tag{7}$$

where the error brackets indicate the 90% confidence intervals for the intercept and slope, if St_* is randomly sampled from a normal distribution (Bowker and Liebermann 1959). At the 90% confidence level the slope is not significantly different from zero (the correlation coefficient is -0.20) and any dependence on Reynolds number is weak, a conclusion reinforced by earlier measurements with much higher Re_* that indicated values for St_* exceeding 5×10^{-3}. The mean value of St_* is 5.6×10^{-3} with standard deviation 1.3×10^{-3}. Mean values of St_* for each drift station considered separately are 0.0055 for the WRS and 0.0057 for Maud Rise, with much larger scatter at the former site.

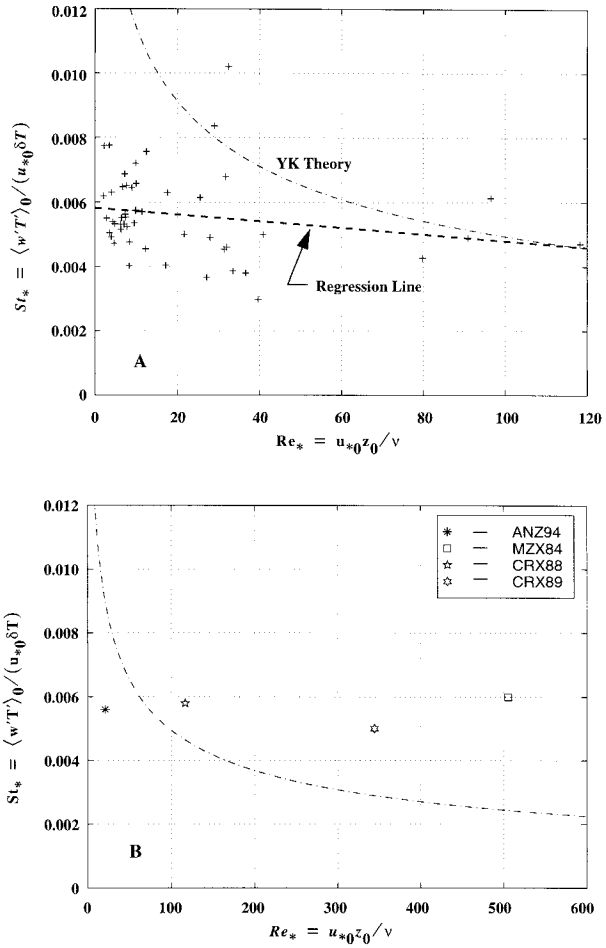

FIG. 6. (a) Scatter diagram of Stanton number (heat exchange coefficient based on friction speed) against surface friction Reynolds number. The slope of the regression line is not significant. The curve labeled "YK Theory" shows the predicted dependence according to the theory of Yaglom and Kader (1974) for heat and mass transport over hydraulically rough surfaces. (b) Average values of heat transfer coefficients from four polar projects with direct ocean heat flux measurements, compared with the YK prediction.

These results are of particular interest because the comparatively smooth ice under the ANZFLUX stations places the present observations in a Reynolds number regime significantly lower than previous sites. This is illustrated by the hydraulically rough surface Stanton number dependence (dashed curves in Fig. 6) predicted by the YK theory [see Eq. (8) of McPhee et al. 1987], assuming that the extent of the transition sublayer in their theory is equivalent to the scale of the roughness elements, $30z_0$. In the present Re_* range, the YK theory significantly overestimates the Stanton number. Figure 6b shows average St_*–Re_* relationships for several ice

[2] For completeness, the parameter list should include the molecular thermal diffusivity leading to a second dimensionless group, the Prandtl number. However, the Prandtl number remains nearly constant for conditions where sea ice is present, and its dependency is ignored here.

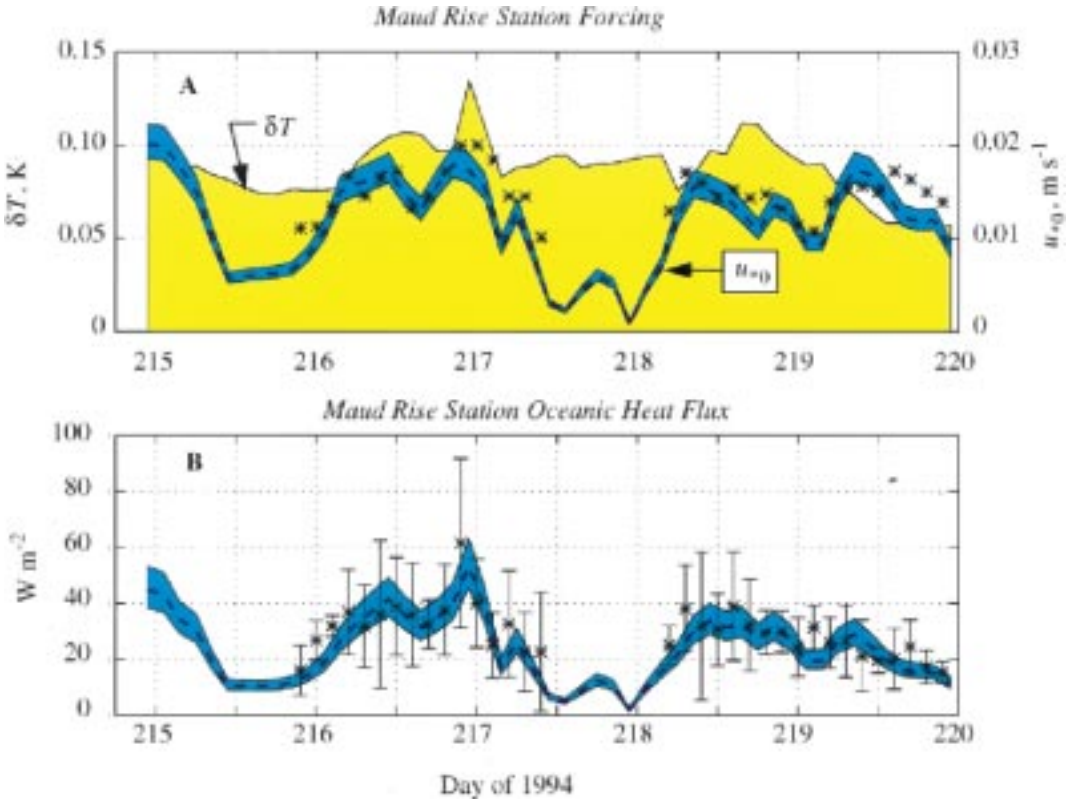

FIG. 7. (a) Mixed layer temperature elevation above freezing (shaded curve) and interfacial friction velocity estimated from Rossby similarity (dashed curve, with envelope showing the range of uncertainty associated with ± one std. dev. of $\log z_0$) for the Maud Rise drift. Asterisks show u_{*0} estimated from turbulence measurements, extrapolated to the surface as described in the text. (b) Ocean-to-ice heat flux based on the bulk exchange model (dashed curve, with envelope showing the range of uncertainty associated with error estimates for both $\log z_0$ and c_H) compared with turbulent heat flux measured with the topmost TIC. Error bars on the measurements represent ± one std. dev. of the 15-min flow realizations in each 2.4-h average.

drift stations from which direct heat flux measurements have been obtained (McPhee 1992). McPhee et al. (1987) noted that in the marginal ice zone (MIZEX84), YK theory underestimated the Stanton number by a factor of ~2, unless the transition sublayer thickness was considerably less than $30z_0$. McPhee (1992) concluded that there was insufficient evidence to warrant using the more complex YK approach instead of constant c_H ($=\mathrm{St}_*$). Here we can make the stronger statement that over the range of roughness Reynolds number likely to be encountered under sea ice, constant c_H is a better choice.

4. Ocean-to-ice heat flux

a. Manned stations

The bulk exchange method for estimating turbulent heat flux (3) was applied with the coefficients established in section 3 ($A = 2.0$, $B = 2.5$, $c_H = 0.0056$) to estimate continuous time series and average values of oceanic heat flux for the manned stations. This serves as both a check on the method and a means of establishing the mean heat flux since turbulence measurements were not always available. For each station, mixed layer temperature and salinity were taken from a mooring-type CT instrument, which continuously recorded 1-min averages one meter below the ice as part of the LMP program (T. Stanton 1996, personal communication). Results are shown first for the Maud Rise station (Fig. 7), where there was a more continuous record of near-surface stress and turbulent heat flux and conditions were less extreme in terms of upper-ocean changes due to drift over eddy features (McPhee et al. 1996). In the upper panel, the shaded curve labeled "u_{*0}" represents friction speed calculated with (2) using the range of $\log z_0$ determined in section 3a. Asterisks mark the values inferred from the near-surface TIC measurements of Reynolds stress. The lower panel similarly shows a range of computed bulk-model heat flux, (3), made by combining the range in u_{*0} (corresponding to ± one std. dev. of $\log z_0$) with the confidence limits for the intercept in the regression of Fig. 5a, applied to the mean value for c_H. Measured heat flux follows the envelope reasonably well. Error bars on the measurements

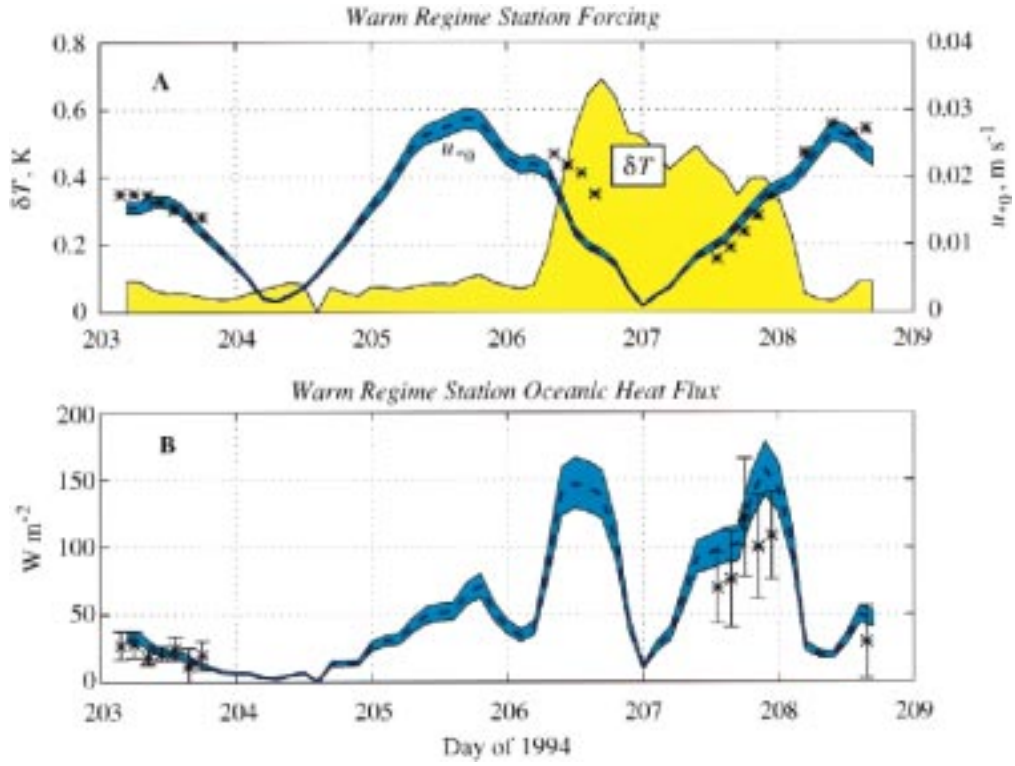

FIG. 8. As in Fig. 7 except for the WRS drift.

indicate the variability in 15-min realizations of the turbulent flow. Mean oceanic heat flux for the 5 days was 23.4 (±4.3) W m^{-2}. Over Maud Rise, the mixed layer temperature rarely departed by more than one-tenth of a degree from freezing, and surface stress was generally less than 0.5 Pa.

Conditions for the WRS were more extreme (Fig. 8): maximum mixed layer temperature reached 0.7 K above freezing and ocean surface stress approached 1 Pa during two gales. According to the bulk model, mean heat flux for slightly more than 5 days was 51.5 (±6.7) W m^{-2}, more than twice the Maud Rise average. There were fewer near-surface data with which to compare the bulk predictions, and the comparison is not so favorable. The large thermal anomaly from day 206 to 208 came when the station drifted onto a warm eddy as the first storm abated. Within a few hours the pycnocline shoaled from 140 to 40 m. Although stratified by rapid melting, the boundary layer remained extremely turbulent as indicated by how much the observed values of u_{*0} on day 206 exceeded the Rossby similarity predictions (as previously discussed, there were also anomalously high values of z_0 for this period, labeled *b* in Fig. 5). In the 9.6 h represented by the four samples on day 206, mean turbulent heat flux was 287 and 436 W m^{-2}, at 3.8 and 6.8 m below the interface, respectively. These far exceed the bulk predictions and are not plotted. If the gradient in boundary layer heat flux implied by the difference between the two clusters is extended linearly to the interface, the mean surface value was about 100 W m^{-2}, which is somewhat less than the bulk prediction. A gradient in heat flux would result from cooler water near the surface advecting with the ice, absorbing much of the upward flux from below as the water warmed.

The station stalled over the eddy between storms. Interestingly, some of the smallest heat flux values predicted by the bulk model occurred near time 207.0, despite mixed layer temperature elevation of 0.5 K. Currents during this time were too small to make valid turbulence measurements, but small heat flux was corroborated by abrupt cessation of ice bottom melting (see Fig. 7 of McPhee et al. 1996). As the wind increased early on day 208, the station drifted off the eddy, and apparently a complementary process occurred: warmer water advected in the upper boundary layer created a positive temperature gradient with *downward* heat flux despite mixed layer temperature still being above freezing. The first three TIC samples on day 208 exhibited negative heat flux.

b. Buoy cluster

A longer time series of ocean-to-ice heat flux was estimated using the buoy speed (from satellite navigation), and temperature and salinity measured with the topmost mooring Seacat, nominally at 10-m depth, from the buoy cluster deployed when the WRC manned site was abandoned. Friction speed was determined from (2)

assuming sea surface tilt was negligible and that z_0 remained near the mean value during the manned drift, 2.2 mm. Temperature elevation and friction speed (Fig. 9a) show that conditions encountered during the WRC manned drift were not grossly anomalous: there were two other storms with u_{*0} reaching 0.03 m s^{-1} and several occasions where mixed layer temperature exceeded 0.3 K above freezing (though none as high as 0.7 K). In Fig. 9b, the heavy horizontal dashed line represents the mean value, 27.4 W m^{-2}, for the first 76 days (30 Jul to 14 Oct 1994), with the best estimates of exchange parameters ($z_0 = 2.2$ mm, $c_H = 0.0056$) from the manned stations. The lighter lines represent mean values for the limits described above: $z_0 = 0.5$ mm, $c_H = 0.0052$, implying $\overline{H} = 22.2$ W m^{-2}, and $z_0 = 3.8$ mm, $c_H = 0.006$, implying $\overline{H} = 30.9$ W m^{-2}.

In agreement with Gordon and Huber (1990), there was a general background heat content to the mixed layer ($\delta T \sim 0.08$ K), punctuated with occasional warm bursts. The bursts were not correlated with the storms, which is evident in that the mean heat flux from Fig. 9b (27.4 W m^{-2}) is almost identical to that calculated from the mean values of δT and u_{*0}: 27.7 W m^{-2}.

5. Conductive heat flux

The AWI buoy installation included a thermistor string extending through the ice into the ocean with 23 sensors spaced 10 cm apart. The upper seven thermometers matched air temperature closely and are presumed to have remained above the snow and ice level, while the lower ten measured very close to water temperature. The thermistor string buoy quit transmitting data on day 259. Figure 10a shows a perspective view of the thermal state of the ice as a function of time and distance from the top of the thermistor string. Thermistors at 130 cm (thermistor 14) and lower showed little variability, reflecting mixed layer temperature, while thermistor 7 at 60 cm followed the air temperature (blue shading) closely. For the first 25 days, temperatures at thermistors 7 (60 cm) and 8 (70 cm) were close to each other and to the air temperature. About day 237 they began to diverge, indicating that thermistor 8 had been enveloped either in fresh snow, or in surface freezing from flooding, as had been observed during storms at the manned stations (Ackley et al. 1995). A contour plot (Fig. 10b) shows that between days 235 and 240, the entire ice column below sea level (assuming 7–8 cm of freeboard) reached temperatures above -5°C. Based on percolation theory, K. Golden (1996, personal communication) has identified a critical brine volume associated with a temperature around -5.3°C as necessary for the permeability of sea ice to water; hence the possibility exists of surface flooding.

Vertical heat conduction within the ice is proportional to the vertical temperature gradient, which was estimated at the level of thermistor 11 (roughly 40 cm below the upper ice surface) from the difference between temperature at thermistors 10 and 12. This level was chosen because it was far enough from the upper surface to be somewhat insulated from large swings in air temperature (and associated changes in ice heat content), yet far enough from the bottom so that the temperature was usually well below freezing. Thermal diffusivity was estimated using the formula of Untersteiner (1961):

$$k_s = k_i + \frac{\beta S_{\text{ice}}}{T}, \tag{8}$$

where k_i is thermal conductivity of pure ice, 2.04 J m^{-1} K^{-1} s^{-1}; S_{ice} is ice salinity on the practical salinity scale, T is ice temperature in °C; and β is constant, 0.1173 J m^{-1} s^{-1}. Temperature was obtained from thermistor 11. Ice salinity was estimated to be 6 psu (S. Ackley 1996, personal communication). The thermistor string was assumed to have equilibrated with its surroundings by day 215. The resulting conductive ice heat flux is compared in Fig. 11 with ocean heat flux, similarly bin-averaged in 1-day increments for the period 215–259. Mean values over the 44-day period turn out to be almost exactly the same: 30 W m^{-2}, which implies that there was little net growth or ablation at the bottom of the ice. However, there are often periods of several days when they are out of balance by tens of watts per square meter, including the period from day 255 to 260 when there must have been quite rapid bottom melting. We can only conjecture whether this event was related to the failure of the thermistor buoy.

6. Summary

Findings from this study may be summarized as follows:

1) The undersurface friction velocity (a vector with magnitude equal to the square root of undersurface kinematic stress and in the same direction) can be adequately estimated from ice drift velocity using a Rossby-similarity relationship (2) with parameters similar to those found for multiyear pack ice in the Arctic. In the seasonal ice of the Weddell Sea, however, the undersurface roughness length z_0 is smaller by as much as two orders of magnitude. Estimated mean values of z_0 for the Warm Regime and Maud Rise manned stations were 2.2 and 1.3 mm, respectively.
2) The heat exchange coefficient (a Stanton number based on friction speed) averaged 0.0056 for the two manned stations. This is within 10% of the value found previously for multiyear pack ice in the Arctic. Dimensional analysis shows no significant dependency on Reynolds number formed from the dimensionless group $u_{*0}z_0/\nu$; thus these results are at odds with laboratory studies of heat and mass transfer over hydraulically rough surfaces showing an inverse square root Reynolds number dependency.
3) At the manned ANZFLUX drift stations, where tur-

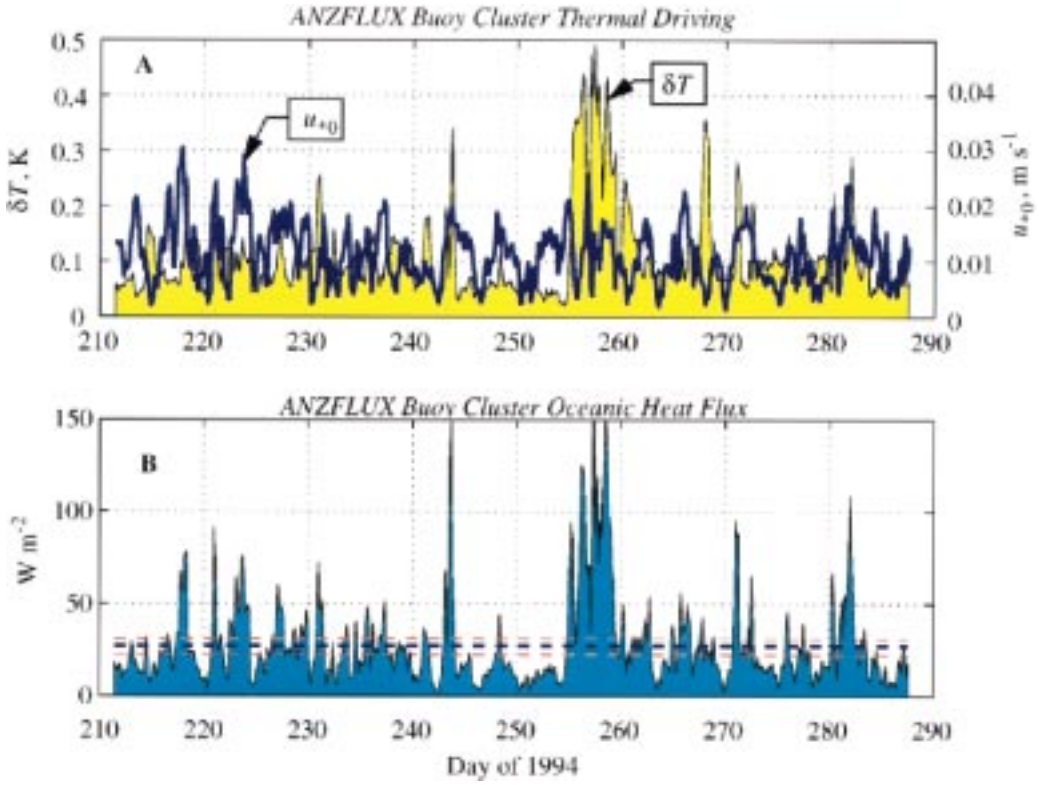

FIG. 9. (a) Friction velocity estimated from the buoy drift speed (solid curve) and temperature elevation above freezing from the topmost *T/C* pair (shaded curve). (b) Ocean-to-ice heat flux from the bulk model (shaded curve). The heavy dashed line is the mean heat flux value (27.4 W m^{-2}) between high and low estimates of the mean associated with errors described in the text.

bulent heat flux and Reynolds stress were measured directly and used to establish bulk exchange coefficients, oceanic heat flux averaged 52 and 23 W m^{-2} for the Warm Regime and Maud Rise stations, respectively. Much of the enhanced heat flux at the WRS occurred over a warm eddy.

4) The unmanned data buoy cluster demonstrated that ocean heat flux in the central Weddell Sea, in the region west and north of Maud Rise, is highly variable. Over the initial 76-day record considered here, ocean heat flux averaged 27 W m^{-2}.
5) Average conductive heat flux in the lower part of the ice column was nearly equal to the mean ocean heat flux during the first 45 days of the buoy drift, implying very little net ice growth or ablation. On shorter timescales there is often an imbalance of tens of watts per square meter, suggesting that the ice grows and melts continuously in response to both ocean heat flux events and atmospheric variation.

Our results confirm that heat flux from the ocean below the well mixed layer largely determines the character of the seasonal ice cover in the Weddell Sea. Throughout winter ice growth is severely restricted by the required venting of 25–35 W m^{-2} upward through the mixed layer. This is accomplished by repeated cycles of bottom melting and freezing, in which the ice cover serves as a thermal ''flywheel,'' maintaining a relatively constant loss to the atmosphere despite large swings in oceanic heat flux from below. As the diminished winter pack encounters polar sunrise, it is far more susceptible to albedo feedback, thus oceanic heat flux may affect the overall energy balance to a greater degree than would be inferred from the sensible heat exchange alone.

The sea ice regime in the Weddell gyre contrasts sharply with the perennial ice pack in the Arctic. There most of the oceanic heat flux occurs during summer from solar heating through leads and thin ice (Maykut and McPhee 1996). Over the deep basins in the Arctic, a cold, stable halocline separates the mixed layer from the main source of oceanic heat, pushing most of the oceanic heat loss to the peripheral seas. Given these differences, and the apparent importance of sea ice in the overall climate picture, it seems reasonable to recommend long term and widespread monitoring of ice–ocean heat exchange. The ANZFLUX results suggest how this can be done by coupling occasional periods of intense sampling with relatively simple and inexpensive measurements, all within a reasonable theoretical framework.

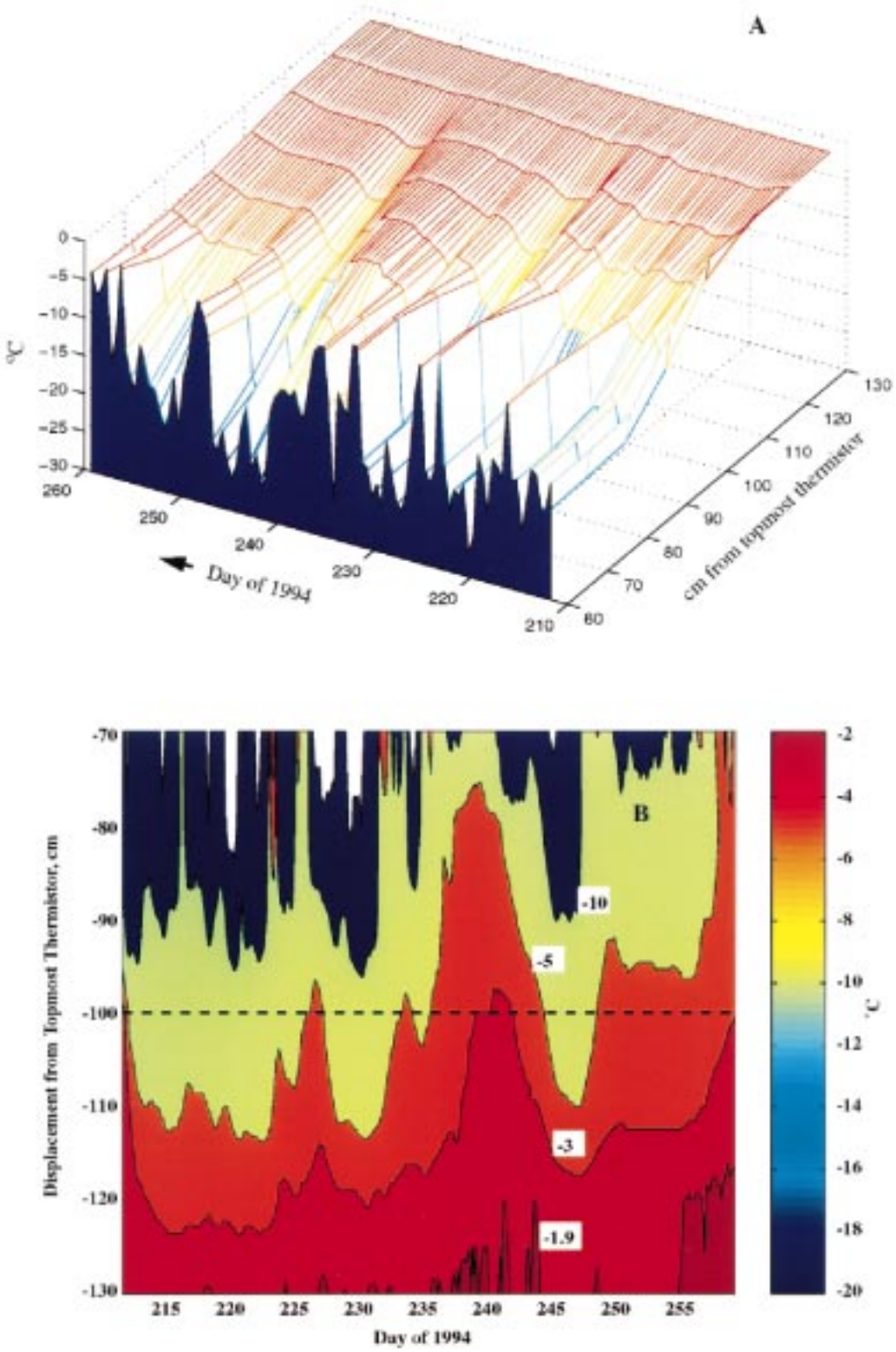

FIG. 10. (a) Perspective view of temperature within the sea ice at the buoy cluster site as a function of distance from the uppermost thermistor and time, from the AWI ice thermistor array. The blue shaded curve is air temperature. (b) Contour representation of ice temperature, showing the level at which the thermal gradient was calculated for estimating conductive heat flux.

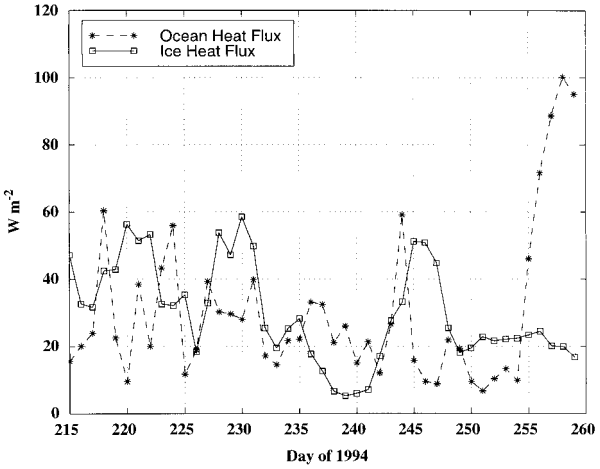

FIG. 11. A comparison of ocean-to-ice heat flux with conductive flux in the ice cover for the period when the ice thermistor array was operational. Mean values are nearly identical: 30 W m^{-2}.

Acknowledgments. We are indebted to T. Stanton for providing the LMP and Maud Rise SeaCat data, and to J. Ardai and T. Lehman for help with the field program. The Alfred Wegener Institute for Polar and Marine Research, Bremerhaven, contributed oceanographic and meteorological buoys to the ANZFLUX experiment. Thanks are due L. Sellman for the processing of AWI buoy data. Funding was provided by the National Science Foundation through Grants OPP 9315920 (MGM), OPP9316958 and OPP9615154 (JHM) and by the Office of Naval Research through Contracts N00014-94-C-0023 and N00014-96-C-0032 (MGM).

REFERENCES

Ackley, S. F., V. I. Lytle, K. M. Golden, M. N. Darling, and G. A. Kuehn, 1995: Sea-ice measurements during ANZFLUX. *Ant. J. U.S.*, **30,** 133–135.

Barenblatt, G. I., 1996: *Scaling, Self-Similarity, and Intermediate Asymptotics.* Cambridge University Press, 386 pp.

Bowker, A. H., and G. J. Lieberman, 1959: *Engineering Statistics.* Prentice-Hall, 585 pp.

Carsey, F., 1980: Microwave observations of the Weddell Polynya. *Mon. Wea. Rev.*, **108,** 2032–2044.

Gill, A. E., 1973: Circulation and bottom water production in the Weddell Sea. *Deep-Sea Res.*, **20,** 111–140.

Gordon, A. L., 1978: Deep Antarctic convection of Maud Rise. *J. Phys. Oceanogr.*, **8,** 600–612.

——, 1982: Weddell Deep Water variability. *J. Mar. Res.*, **40,** 199–217.

——, 1991: Two stable modes of Southern Ocean winter stratification. *Deep Convection and Deep Water Formation in the Oceans,* P.-C. Chu and J.-C. Gascard, Eds., Elsevier Oceanogr. Ser., Vol. 57, Elsevier, 17–35.

——, and B. Huber, 1984: Thermohaline stratification below the Southern Ocean sea ice. *J. Geophys. Res.*, **89,** 641–648.

——, and ——, 1990: Southern Ocean winter mixed layer. *J. Geophys. Res.*, **95,** 11 655–11 672.

Lemke, P., W. B. Owens, and W. D. Hibler III, 1990: A coupled sea ice–mixed layer–pycnocline model for the Weddell Sea. *J. Geophys. Res.*, **95,** 9513–9525.

Levine, M. D., L. Padman, R. D. Muench, and J. H. Morison, 1997: Internal waves and tides in the western Weddell Sea: Observations from Ice Station Weddell. *J. Geophys. Res.*, **102,** 1073–1089.

Martinson, D. G., 1990: Evolution of the Southern Ocean winter mixed layer and sea ice: Open ocean deep water formation and ventilation. *J. Geophys. Res.*, **95,** 11 641–11 654.

——, P. D. Killworth, and A. L. Gordon, 1981: A convective model for the Weddell Polynya. *J. Phys. Oceanogr.*, **11,** 466–488.

Maykut, G. A., and N. Untersteiner, 1971: Some results from a time-dependent thermodynamic model of sea ice. *J. Geophys. Res.*, **76,** 1550–1575.

——, and M. G. McPhee, 1995: Solar heating of the Arctic mixed layer. *J. Geophys. Res.*, **100,** 24 691–24 703.

McPhee, M. G., 1979: The effect of the oceanic boundary layer on the mean drift of sea ice: Application of a simple model. *J. Phys. Oceanogr.*, **9,** 388–400.

——, 1990: Small scale processes. *Polar Oceanography,* W. Smith, Ed., Academic Press, 287–334.

——, 1992: Turbulent heat flux in the upper ocean under sea ice. *J. Geophys. Res.*, **97,** 5365–5379.

——, 1994: On the turbulent mixing length in the oceanic boundary layer. *J. Phys. Oceanogr.*, **24,** 2014–2031.

——, 1999: Scales of turbulence and parameterization of mixing in the ocean boundary layer, *J. Fluid Syst.*, in press.

——, and D. G. Martinson, 1994: Turbulent mixing under drifting pack ice in the Weddell Sea. *Science,* **263,** 218–221.

——, and T. P. Stanton, 1996: Turbulence in the statically unstable oceanic boundary layer under Arctic leads. *J. Geophys. Res.*, **101,** 6409–6428.

——, G. A. Maykut, and J. H. Morison, 1987: Dynamics and thermodynamics of the ice/upper ocean system in the marginal ice zone of the Greenland Sea. *J. Geophys. Res.*, **92,** 7017–7031.

——, S. F. Ackley, P. Guest, B. A. Huber, D. G. Martinson, J. H. Morison, R. D. Muench, L. Padman, and T. P. Stanton, 1996: The Antarctic Zone Flux Experiment. *Bull. Amer. Meteor. Soc.*, **77,** 1221–1232.

Owen, P. R., and W. R. Thompson, 1963: Heat transfer across rough surfaces. *J. Fluid Mech.*, **15,** 321–334.

Schlosser, P., R. Bayer, A. Foldvik, T. Gammelsrod, G. Rohardt, and K. O. Munnich, 1990: Oxygen 18 and Helium as tracers of ice shelf water and water/ice interaction in the Weddell Sea. *J. Geophys. Res.*, **95,** 3253–3264.

Stanton, T. P., 1995: Mixed layer structure and turbulent fluxes in the eastern Weddell Sea during the ANZFLUX experiment. *Ant. J. U.S.*, **30,** 124–125.

Untersteiner, N., 1961: On the mass and heat budget of Arctic sea ice. *Arch. Meteor. Geophys. Bioklimatol. Ser. A,* **12,** 151–182.

Wadhams, P., M. Lange, and S. F. Ackley, 1987: The ice thickness distribution across the Atlantic sector of the Antarctic Ocean in midwinter. *J. Phys. Res.*, **92,** 14 535–14 552.

Washington, W. M., A. J. Semtner, C. Parkinson, and L. Morrison, 1976: On the development of a seasonal change sea ice model. *J. Phys. Oceanogr.*, **6,** 679–685.

Yaglom, A. M., and B. A. Kader, 1974: Heat and mass transfer between a rough wall and turbulent flow at high Reynolds and Peclet numbers. *J. Fluid Mech.*, **62,** 601–623.

Zwally, H. J., and P. Gloersen, 1977: Passive microwave images of the polar regions and research application. *Polar Rec.*, **18,** 431–450.